Metallophysics and Advanced Technologies
Металофіз. новітні технол.
Metallofiz. Noveishie Tekhnol.
2025, vol. 47, No. 10, pp. 1111–1123
https://doi.org/10.15407/mfint.47.10.1111
Reprints available directly from the publisher

PACS numbers: 61.05.cp, 61.72.Ff, 62.20.fg, 62.20.fk, 62.20.Qp, 68.37.Hk, 81.20.Ev

Microstructure, Phase Evolution, and Mechanical Properties of CoCrNi. Medium-Entropy Alloy Processed by Powder Metallurgy Techniques

M. G. Salazar-Juárez[*], I. Estrada-Guel[**], C. Gamaliel Garay-Reyes[**], C. D. Gómez-Esparza[***], R. Martínez-Sánchez[**], J. A. Castillo-Robles[*], C. A. Calles-Arriaga[*], E. Rocha-Rangel[*]

[*]*Universidad Politécnica de Victoria,*
5902 New Technologies Ave.,
87138 Ciudad Victoria, Tamaulipas, México
[**]*Centro de Investigación en Materiales Avanzados,*
120 Miguel de Cervantes,
31136 Chihuahua, Chi, México
[***]*Universidad Autónoma de Chihuahua,*
900 Escorza Ave.,
31000 Chihuahua, Chih., México

CoCrNi alloys are a new family of high-performance alloys, which have found use in a variety of applications, including automotive, aerospace, and biomedical industries. The alloys can be manufactured by different processes, and they offer excellent properties such as high strength, good ductility, biocompatibility, and corrosion resistance. This article discusses the manufacturing route, phase evolution, and mechanical properties of medium-entropy CrCoNi-based alloys processed by means of powder-metallurgy techniques. Some of the main results obtained indicate that there is the presence of a Co–Cr–Ni solid solution and a mixture of f.c.c. and b.c.c. structures in the alloy. The microstructure is homogeneous with equiaxial grains and con-

Corresponding author: Enrique Rocha-Rangel
E-mail: erochar@upv.edu.mx

Citation: M. G. Salazar-Juárez, I. Estrada-Guel, C. Gamaliel Garay-Reyes, C. D. Gómez-Esparza, R. Martínez-Sánchez, J. A. Castillo-Robles, C. A. Calles-Arriaga, and E. Rocha-Rangel, Microstructure, Phase Evolution, and Mechanical Properties of CoCrNi. Medium-Entropy Alloy Processed by Powder Metallurgy Techniques, *Metallofiz. Noveishie Tekhnol.*, **47**, No. 10: 1111–1123 (2025), DOI: 10.15407/mfint.47.10.1111

tains a mixture of phases due to the alloying elements. The alloy presents high mechanical strengths with good strain values. The presence of different phases, between them a Co–Cr–Ni solid solution and Co–Ni one with dissimilar crystalline structures, is the cause of the high entropy of the alloy and, consequently, of its good mechanical characteristics.

Key words: Co–Cr–Ni alloy, medium entropy alloys, solid solutions, f.c.c. and b.c.c. structures, mechanical properties.

Стопи CoCrNi — це нове сімейство високоефективних стопів, які знайшли застосування в різних сферах, включаючи автомобільну, аерокосмічну та біомедичну промисловості. Стопи можуть бути виготовлені різними методами та демонструють відмінні властивості, такі як висока міцність, пластичність, біосумісність і корозійна стійкість. У цій статті розглянуто технологічний процес виготовлення, еволюцію фаз і механічні властивості середньоентропійних стопів на основі CrCoNi, оброблених методами порошкової металургії. Деякі з основних одержаних результатів вказують на наявність твердого розчину Co–Cr–Ni і суміші ГЦК- й ОЦК-структур у стопі. Мікроструктура є однорідною з рівновісними зернами та містить суміш фаз через леґувальні елементи. Стоп демонструє високу механічну міцність з хорошими значеннями деформації. Наявність різних фаз, серед яких — тверді розчини Co–Cr–Ni та Co–Ni з несхожими кристалічними структурами, є причиною високої ентропії стопу і, відповідно, його хороших механічних характеристик.

Ключові слова: стоп Co–Cr–Ni, середньоентропійні стопи, тверді розчини, ГЦК- й ОЦК-структури, механічні властивості.

(Received 12 October, 2024; in final version, 1 April, 2025)

1. INTRODUCTION

High-entropy alloys (HEAs) or multicomponent alloys are made up of several main elements (more than five), which generally have an equiatomic or close to equiatomic composition. Cantor and Yeh first reported in 2004 on this type of alloys working separately [1, 2]. All alloys in use today, contain a high proportion of one element with minor amounts of additional elements added, but HEAs are made of an equal mixture of each constituent element. These balanced atomic compositions appear to give some of these materials an extraordinarily high combination of strength and ductility when subjected to stress, which together form what is called ‘toughness’. The composition of these new alloys theoretically provides practically limitless possibilities for the design of the composition and optimization of alloy properties. Due to the high entropy of their structure, HEAs are recognized to present larger physical, chemical, and mechanical properties compared to conventional alloys, including exceptional thermal stability, corrosion resistance and, high fracture toughness [3–8]. Even some of

the alloys developed have excellent magnetic properties [9, 10]. Thus, HEAs have been a hot field of research since they were first developed just over 20 years ago. However, several authors have reported that HEAs are multiphase alloys [11–14], which causes their entropy to be not so high. Moreover, only a few of the many HEAs until now studied are single-phase solid solutions. Thus, the number of components of the alloy is not most important factor, and the chemical nature of the components must be critically studied. Given this situation, about 10 years ago, medium entropy alloys (MEAs) began to be developed, which are made up of 3 elements added as in HEAs in equiatomic quantities or close to them, with the idea of obtaining in these alloys a single-phase solid solution with the 3 alloying elements. Among the medium entropy alloys studied, it is found that the CrCoNi alloys are a family of high-performance alloys that have found use in a diversity of applications, including aerospace, biomedical, and automotive industries. The alloys are formed by combining chromium, cobalt, and nickel, and they offer excellent properties such as high strength, ductility, biocompatibility, and corrosion resistance. For these reasons, this alloy has been extensively studied, trying to understand the mechanisms of seeking to explain the reasons for its high properties [15–18]. Likewise, Zhang *et al.* [19] studied the short-range order and exposed that it plays an important role in lowering the electrical and thermal conductivities in the alloy. Other researchers have conducted studies that include grain refinement [20], heterogeneous structure [21], and the effect of alloying elements [22–25], oriented to determine the relationships between strength and ductility. Finally, oxidation resistance and biocompatibility have also been explored [26]. In summary, it has been established that MEAs possess excellent microstructures and properties, which can be compared with or even better than those of HEAs can. Therefore, its study is of great interest. The objective of this work is to produce by powder metallurgy the CrCoNi equiatomic alloy and to study the mechanical and microstructural response of the alloy subjected to different heat treatments).

2. MATERIALS AND METHODS

Elemental powders of Cr, Co, and Ni with purity greater than 99% and sizes of –325 mesh, in equiatomic proportions, were mechanically processed in a high-energy planetary mill (Retsch, PM 100, Germany). The grinding parameters used in the mixture were as follows: dry grinding for 6 hours at 300 rpm, using methyl alcohol as a control agent, and managing a ball weight to powder weight ratio of 10:1. Once the powders were ground, they were pressed to form cylindrical pellets with an average diameter and height of 10 mm and 3 mm respectively, using a tool grade steel die. Compaction of these samples was carried out at

room temperature by uniaxial pressing using a pressure of 300 kg/cm^2 in a hydraulic press (Montequipo, LAB-30T, México). Afterward, all the pellets were sintered in an electric furnace (Carbolite RHF 17/3E, England) at 1400°C for 2 h, with a heating rate of 10°C/min. The furnace was set up with a protective argon atmosphere to prevent oxidation of the metals. In order to determine the effect of different annealing heat treatments on the mechanical properties of the alloy, 3 heat treatments were carried out at 300, 400, and 500°C for 1 hour each, on the already sintered samples. After the grinding stage, the particle size distribution and the specific surface area were determined using a Mastersizer 2000 equipment of English origin. Before characterization of the sintered samples, they were ground with SiC sandpaper and then polished using alumina and diamond suspensions. Crystalline phases of sintered alloys were determined using x-ray diffraction analysis (XRD) under CuK_α radiation, performed on X'Pert PRO PANalytical and interpreted with the X'Pert Highscore Plus PANalytical software using patterns in the ICDD PDF2 database. Meanwhile, scanning electron microscopy (SEM) and an energy dispersion spectrometer detector (EDS) on a HITACHI SU3500 microscope analysed the obtained microstructure. Microstructure after annealing treatments was analysed by optical microscopy (Nikon 2000 plus, Japan). Finally, the study samples were characterized to determine the mechanical properties. The mechanical properties evaluated were as follows: The ultrasonic method determined Young's modulus, following ASTM standards [27], using Grindosonic A-360 Japanese manufacturing equipment. Microhardness was evaluated in agreement with the ASTM E384–16 standard [28]. In this case, twelve measurements were performed at different sample locations and the average value of the indentations is reported; these measurements were performed with a microhardness tester (Wilson Instruments Model S400, USA). The compressive strength was evaluated at a Universal Material Tester WP 300 Gunt, German).

3. RESULTS AND DISCUSSION

3.1. Particle Size

Figure 1 shows the distribution of particle sizes obtained after powder grinding. This figure shows a good distribution of powder, with sizes ranging from 5 microns to approximately 17 microns. Results show that 50% of the powders are smaller than 9.5 microns, while 25% of them are smaller than 8 microns. This distribution of powder sizes can be considered well because, during the powder compaction stage, it will be feasible to arrange the powders in such a way that the spaces left by the larger powders will be occupied by the smaller ones, thus causing a high number of contacts between the powders and a higher densifica-

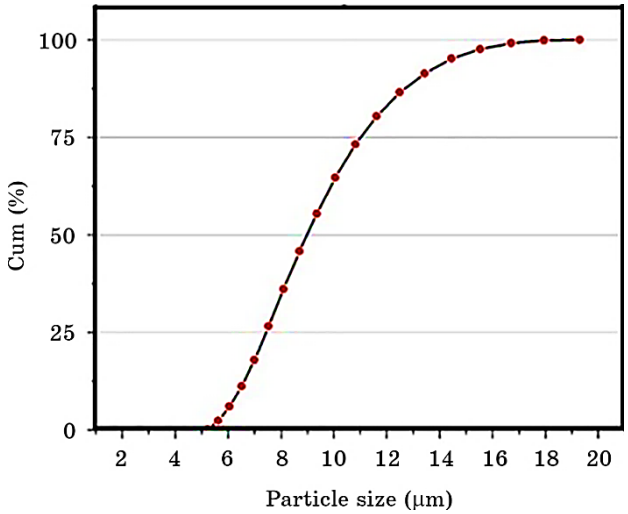

Fig. 1. Particle size distribution of the grinded mixture.

tion of the green sample. These two conditions will favour the densification of the sample during the sintering stage.

3.2. Phase Analysis

The x-ray diffraction pattern from metallic components present in the sintered sample is shown in Fig. 2. In this diffraction pattern, it can be observed at angles 2 theta of 43.3°, 54.1°, and 74.4° that some solid solution phases have formed due to the combination of the 3 elements of the alloy (Co, Cr, and Ni). In agreement with that reported by Guo *et al.* [29], the crystal structure in the peaks where the 3 metals of the alloy were mixed corresponds to a cubic structure centred on the faces. Also, at angles of 57.7°, it can be observed that another phase is formed between Ni and Co. Owing to this, there is the presence of a mixture of face-centred cubic (f.c.c.) by the presence of Ni and body-centred cubic (b.c.c.) crystalline structures in those regions where the Ni and Co were combined. The pattern shows some peaks corresponding to the original unmixed metals. This may be mainly due to the high melting point of chromium as well as its larger atomic radius compared to the other two metals nickel and cobalt. Hence, it is also understandable why nickel and cobalt can be properly mixed to form a solid solution. The mixture of these phases with different crystalline structures states the high entropy of the alloy. In order to obtain a single solid solution with a unique phase, it is recommended for future studies to sinter samples at higher temperatures (1.500°C), to dissolve chromium in the structure of the other 2 metals. Nevertheless, with the presence

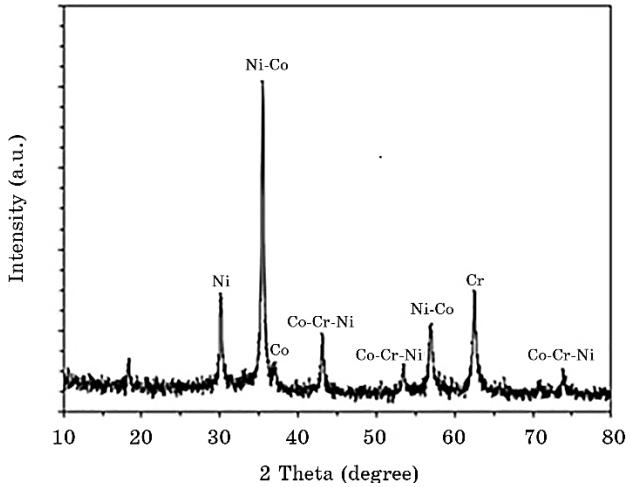

Fig. 2. X-ray diffraction patter of the sintered sample.

of different crystalline structures and two phases, it can be expected that the alloy may have a good combination of mechanical properties such as high hardness and elastic modulus combined with good mechanical strength and ductility.

3.3. Microstructure (SEM)

Figure 3 shows a scanning electron microscope photograph taken at two different magnifications of a representative sample of the alloy microstructure after sintering. Here, we can better observe the morphology and size of the grains, which, is equiaxial with varied sizes. The presence of very small pores in intergranular zones can also be appreciated. From this figure, it can be commented that the alloy was densified very well during the sintering stage, so a good mechanical response could be expected from it.

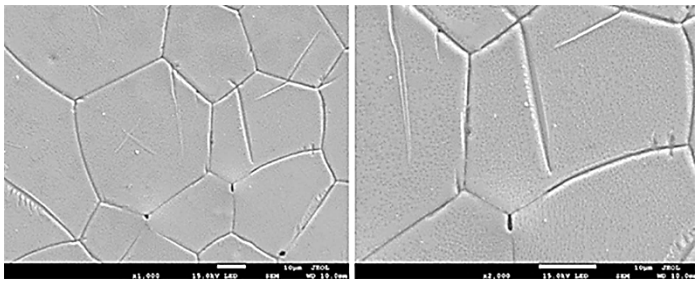

Fig. 3. Microstructure of sintered sample observed with SEM.

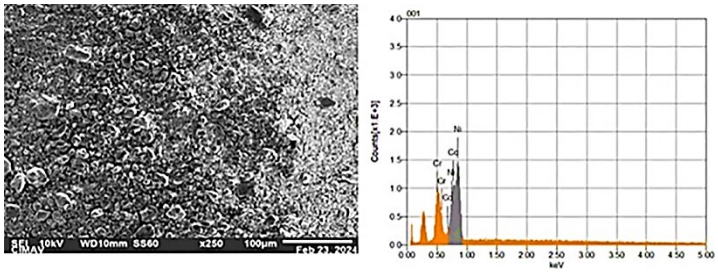

Fig. 4. Energy dispersive spectroscopy of x-rays analysis performed on the sintered alloy.

3.4. Energy Dispersive Spectroscopy of X-Rays

To confirm the presence of the alloying elements, an energy dispersive spectroscopy of x-ray analysis was performed on the sintered alloy. The result of this analysis is shown in Fig. 4, where it can be observed that the spectrum shows the presence of the three main components of the alloy Co, Cr, and Ni. This confirms that the sample was not contaminated or oxidized during processing.

3.5. Mapping

Figure 5 shows a typical mapping of the elements in the alloy. This elemental analysis mapping shows that the sample exhibits that sintered CoCrNi alloy possesses multiphase microstructures. In the figure, spatial areas with a good distribution of alloying elements indicate the formation of the entropy alloys sought here. From this analysis, it can be determined that the microstructure of this alloy is composed of a Co, Cr, and Ni solid solution (light areas), and a dark region composed of dispersed nickel–cobalt phases. This composition confirms the observation made in the x-ray diffraction analysis.

3.6. Microstructure after Annealing (OM)

Figure 6 presents the microstructure observed by optical microscopy of the annealing samples. In this image, it can be observed in all pictures that microstructure is characterized by the presence of equiaxial grains with a size distribution. Depending on the treatment temperature, grain coarsening is observed, which is greater at higher treatment temperatures. The presence of grains larger than 20 microns is observed in the sample annealed at 500°C, whereas, in the sintered sample and that treated at 300°C, the grain size does not exceed 10 microns. This is indicative of the fact that high treatment temperatures

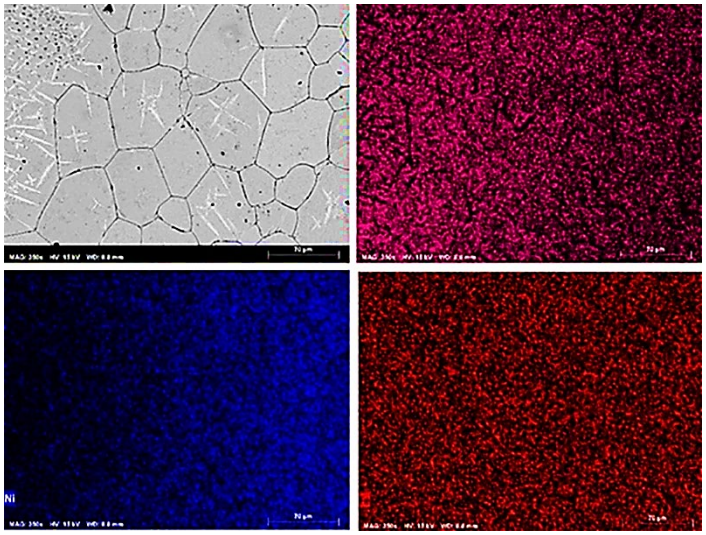

Fig. 5. Mappings performed by energy dispersive x-ray spectroscopy on the medium entropy alloy to verify the distribution of the alloy components.

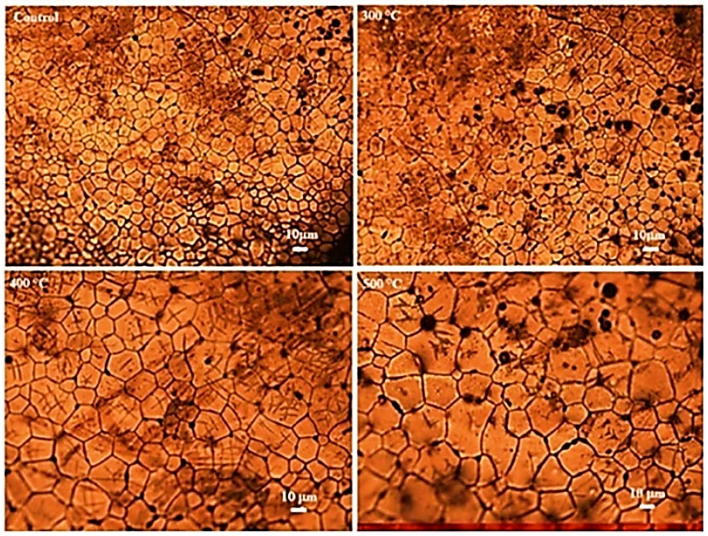

Fig. 6. Microstructure of sintered and heat-treated samples observed with optical microscope.

cause uncontrolled growth of the microstructure, which may affect its mechanical behaviour.

Some porosity is observed in the samples, with small pores (less than 1 micron) for the sintered sample and bigger pores in the sample treat-

ed at 500°C. The porosity in all samples is located mainly in intergranular zones. Due to grain growth, it is not expected that samples treated at elevated temperatures present the best mechanical properties because there are fewer barriers (grain boundaries) to prevent the advancement of cracks generated during stress application.

3.7. Mechanical Properties

For comparative purposes, the mechanical properties evaluated in the alloy heat-treated at different temperatures are compared with those of quenched and tempered AISI 4140 steel. AISI 1040 steel is a low alloy steel of the Cr–Mo series, which has high strength and hardenability, good toughness, high creep resistance and long-lasting high-temperature resistance. This steel has many uses in the aerospace, oil and gas, and automotive industries. Typical uses are thin-walled pressure vessels, forged gears and shafts, spindles, high-strength bolts, and torsion bars [30].

3.7.1. Elastic Modulus

Figure 7 shows the values of the elastic modulus in the heat-treated alloy. This figure initially shows a slight increase in the modulus of the sample treated at 300°C compared to the control sample (untreated), then at higher treatment temperatures, the elastic modulus decreases considerably. This may be due to the coarsening of the microstructure due to the treatment temperatures, where probably also with abnormal grain growth, the porosity increased causing a loss of rigidity of the alloy. The value of the elastic modulus of the AISI4140 steel is well above the values of the Co–Cr–Ni alloy processed here. This is because this steel was first manufactured by casting and then cold-deformed and heat-treated; so, there was good control of the microstructure of the steel at each stage of processing.

3.7.2. Hardness

Figure 7 also shows the microhardness values of the Co–Cr–Ni alloy. The figure shows an analogous behaviour to the elastic modulus, with an increase in the sample treated at 300°C and a considerable drop in hardness at higher treatment temperatures. However, when comparing the hardness values of the alloy treated at 300°C with those of the AISI4140 steel, a slightly higher hardness is observed in the alloy than in the AISI4140 steel. This behaviour may be due to the mixture of f.c.c. and b.c.c. crystal structures including the presence in small areas of the compact hexagonal structure due to the chromium that did not

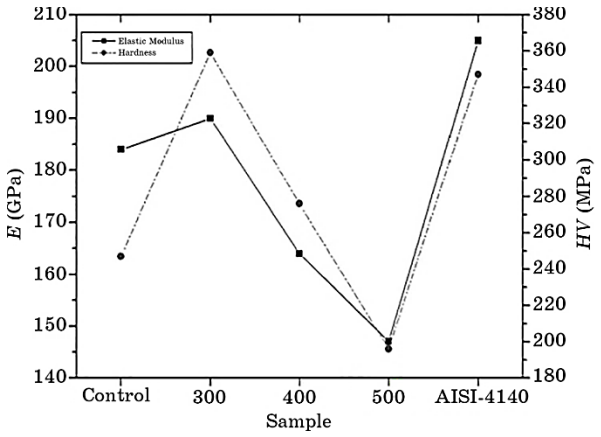

Fig. 7. Elastic modulus and hardness of the Co–Cr–Ni alloy sintered, heat treated and compared with those properties of AISI41440 steel.

dissolve in the alloy. Here the significant increase in the hardness of the sample treated at 300°C compared to that of the control sample is striking. Therefore, the treatment at this temperature probably favoured the recrystallization and the relief of some stresses generated during processing, such as the high mechanical deformation of the metals during milling and later during compaction.

3.7.3. Yield and Compression Strength

Figure 8 shows the results of the yield and compressive strength of the heat-treated Co–Cr–Ni alloy. Again, here, it is observed that the sample treated at 300°C has the highest values of yield and compression strength from all tests, including those of AISI4140 steel. It has been found that high-temperature treatments at 400°C and 500°C result in considerable degradation of the alloys' strength, even dropping below that of the simply sintered sample. As mentioned above, this may be due to the coarsening of the microstructure at these high treatment temperatures. Regarding the higher strength of the alloy compared to AISI4140 steel, the reason is due to the solid solution formed by the alloy elements, the mixture of phases and the combination of crystalline structures, which causes higher entropy and consequently a better mechanical behaviour due to the different sliding systems that are present in the alloy.

3.7.4. Ductility

Figure 9 shows the ductility of the Co–Cr–Ni alloy and that of AI-

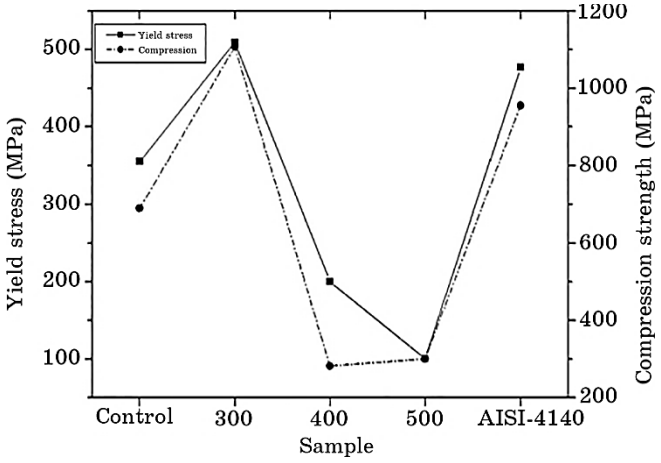

Fig. 8. Yield and compressive strength of the sintered alloy, annealed alloy and compared with those properties of AISI41440 steel.

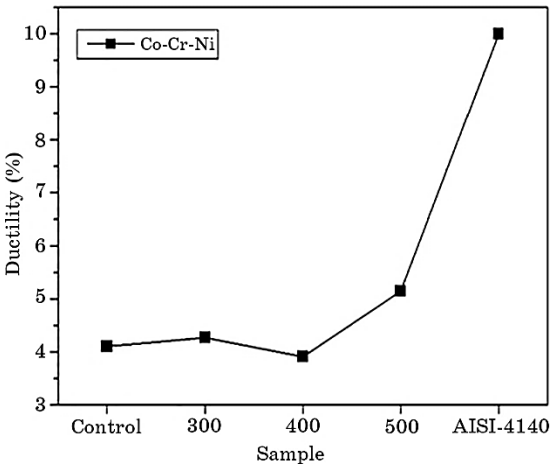

Fig. 9. Ductility of the Co–Cr–Ni alloy and of AISI4140 steel during mechanical compression tests.

SI41440 steel during mechanical compression tests. As expected, an alloy obtained by powder metallurgy will not exhibit considerable ductility values, due to the nature of its microstructure formation, which was obtained through the union of powders. This figure shows similar ductility values between the control sample and the heat-treated samples, which range from approximately 4 to 5%.

While the ductility of AISI steel is more than 100% compared to the ductility of the Co–Cr–Ni alloy, reaching values are slightly higher

than 10%.

This demonstrates the good characteristic of steel that it can combine a number of mechanical properties, significantly improving one without decreasing others. However, having compared the mechanical properties of the alloy manufactured here with those of AISI steel and observing that in some of them the mechanical properties of the Co–Cr–Ni alloy are superior to those of steel, it is indicative that this new alloy has great potential to replace steel in some applications.

4. CONCLUSIONS

The powder metallurgy process has proved to be an effective, cheap, and easy experimental route for the manufacture of medium entropy alloys. Since mechanical milling makes finer particle size and lattice distortion, both conditions facilitate metal bonding in the solid state. Likewise, sintering promotes metal diffusion and, consequently, their solubility and sample consolidation.

Based on XRD studies, it was determined the formation of a mixture of crystalline structures composed of f.c.c. and b.c.c. ones, as well as, the formation of Ni–Cr–Co and Ni–Co solid solution phases.

In order to obtain a single solid solution with a unique phase, it is recommended for future studies to sinter samples at higher temperatures (1 500°C) to dissolve chromium in the structure of the other 2 metals.

The MEA alloy that achieved the better mechanical behaviour is the sample annealed at 300°C, whereas, heat treatment at highest temperatures than 400°C provokes decrement of the mechanical properties of the alloy. The better mechanical properties of the Co–Cr–Ni alloy heat treated at 300°C are due to the mixture of crystalline structures, the formation of solid solutions in the alloy, and recrystallization during the heat treatment.

ACKNOWLEDGEMENTS

M.G.S.J. would like to express their appreciation to CONAHCyT for the grant to carry out her master degree studies.

REFERENCES

1. J. W. Yeh, S. K. Chen, S. J. Lin, J. Y. Gan, T.-S. Chin, T.-T. Shun, C.-H. Tsau, and S.-Y. Chang, *Adv. Eng. Mate.*, **6**, Iss. 5: 299 (2004).
2. B. Cantor, I. T. H.Chang, P. Knight, and A. J. B. Vincent, *Mater. Sci. Eng. A*, **375–377**: 213 (2004).
3. M. Sun, X. Liu, W. Jiang, L. Yawei, K. Jiangang, L. Rui, W. Xianping,

W. Xuebang, F. Qianfeng, and L. Changsong, *Scr. Mater.*, **204**: 114144 (2021).
4. P. Muangtong, A. Rodchanarowan, D. Chaysuwan, N. Chanlek, and R. Goodall, *Corros. Sci.*, **172**: 108740 (2020).
5. D. B. Miracle and O. N. Senkov, *Acta Mater.*, **122**: 448 (2017).
6. G. Bracq, M. Laurent-Brocq, L. Perrière, R. Pirès, J. M. Joubert, and I. Guillot, *Acta Mater.*, **128**: 327 (2017).
7. S. Haas, M. Mosbacher, O. N. Senkov, and M. Feuerbacher, *Entropy*, **20**, Iss. 9: 654 (2018).
8. X. Gao, Y. Lu, B. Zhang, L. Ningning, W. Guanzhong, S. Gang, L. Jizi, and Z. Yonghao, *Acta Mater.*, **141**: 59 (2017).
9. E. P. George, D. Raabe, and R. O. Ritchie, *Nat. Rev. Mater.*, **4**: 515 (2019).
10. S. Singh, N. Wanderka, K. Kiefer, K. Siemensmeyer, and J. Banhart, *Ultramicroscopy*, **111**, Iss. 6: 619 (2011).
11. Z. Tang, M. C. Gao, H. Diao, T. Yang, J. Liu, T. Zuo, Y. Zhang, Z. Lu, Y. Cheng, Y. Zhang, K. A. Dahmen, P. K. Liaw, and T. Egami, *JOM*, **65**: 1848 (2013).
12. Z. Wang, S. Guo, and C. T. Liu, *JOM*, **66**: 1966 (2014).
13. A. Manzoni, H. Daoud, S. Mondal, S.V. Smaalen, R. Völkl, U. Glatzel, and N. Wanderka, *J. Alloys Compd.*, **552**: 430 (2013).
14. S. Singh, N. Wanderka, B. Murty, U. Glatzel, and J. Banhart, *Acta Mater.*, **159**, Iss. 1: 182 (2011).
15. S. Yang, M. Jiang, H. Li, Y. Liu, and L. Wang, *Rare Metals*, **31**: 75 (2012).
16. T. Omori, J. Sato, K. Shinagawa, I. Ohnuma, K. Oikawa, R. Kainuma, and K. Ishida, *J. Phase Equilib. Diffus.*, **35**: 178 (2014).
17. B. Gludovatz, A. Hohenwarter, K. V. Thurston, H. Bei, Z. Wu, E. P. George, and R. O. Ritchie, *Nat. Commun.*, **7**: 10602 (2016).
18. S. Yoshida, T. Bhattacharjee, Y. Bai, and N. Tsuji, *Scr. Mater.*, **134**: 33 (2017).
19. Z. Zhang, H. Sheng, Z. Wang, B. Gludovatz, Z. Zhang, E. P. George, Q. Yu, S. X. Mao, and R. O. Ritchie, *Nat. Commun.*, **8**: 14390 (2017).
20. P. Sathiyamoorthi, J. Moon, J. W. Bae, P. Asghari-rad, and H. S. Kim, *Scr. Mater.*, **163**: 152 (2019).
21. R. Wen, C. You, L. Zeng, H. Wang, and X. Zhang, *J. Mater. Sci.*, **55**: 12544 (2020).
22. W. Lu, X. Luo, Y. Yang, and B. Huang, *Materials Express*, **9**, No. 4: 291 (2019).
23. X. Feng, J. U. Surjadi, R. Fan, X. Li, W. Zhou, S. Zhao, and Y. Lu, *Mater. Today*, **42**, 10 (2021).
24. Y. Shi, Y. Wang, S. Li, R. Li, and Y. Wang, *Mater Sci. Eng. A*, **788**: 139600 (2020).
25. C. Slone, C. Larosa, C. Zenk, E. George, M. Ghazisaeidi, and M. Mills, *Scr. Mater.*, **178**: 295 (2020).
26. M. P. Agustianingrum, U. Lee, and N. Park, *Corros. Sci.*, **173**: 108755 (2020).
27. *ASTM E494-15 Standard Practice for Measuring Ultrasonic Velocity in Materials*, last update (2021).
28. *ASTM E384-16, Standard Test Method for Microindentation Hardness of Materials*, last update (2017).
29. S. Guo, C. Ng, and C. Liu, *J. Alloys Compd.*, **557**: 77 (2013).
30. http://www.acerosespeciales.net/aisi4140.html (last accessed August 29, 2024).